Stabilization of Carbon-Supported Platinum–Rare Earth Nanoalloys during Electrochemical Activation

Carlos Campos-Roldán, Jean-Sébastien Filhol, Hazar Guesmi, Mickaël Bigot, Raphaël Chattot, Andrea Zitolo, Pierre-Yves Blanchard, Jacques Rozière, Deborah Jones, Sara Cavaliere

Stabilization of Carbon-Supported Platinum-Rare Earth Nanoalloys during Electrochemical Activation

Carlos A. Campos-Roldán†, Jean-Sébastien Filhol†, Hazar Guesmi†, Mickaël Bigot†, Raphaël Chattot†, Andrea Zitolo¶, Pierre-Yves Blanchard†, Jacques Rozière†, Deborah J. Jones†, Sara Cavaliere †**

† ICGM, University Montpellier, CNRS, ENSCM, 34095 Montpellier cedex 5, France

¶ Synchrotron SOLEIL, L'Orme des Merisiers, BP 48 Saint Aubin, 91192 Gif-sur-Yvette, France

*Corresponding authors:
carlos-augusto.campos-roldan@umontpellier.fr,
sara.cavaliere@umontpellier.fr

KEYWORDS: Pt alloys, Rare earth metal, *Operando* measurements, Electrochemical activation, Oxygen reduction reaction, Proton exchange membrane fuel cell

ABSTRACT

Carbon-supported platinum-rare earth nanoalloys are promising electrocatalysts for the oxygen reduction reaction. However, their structure-activity-stability trends are poorly understood. Herein, we followed the evolution of Pt-Nd/C nanoalloys during the electrochemical surface conditioning, *i.e.*, prior to the initial evaluation of electrocatalytic activity, and observed that their compositional, morphological and structural *ex situ* properties are considerably modified by the electrochemical activation step. It is these stabilized properties, therefore, that should be considered when discussing the electrocatalyst beginning of life state for the structure-activity-stability relationships rather than those determined *ex situ* on the as-synthesized electrocatalyst.

Proton-exchange membrane fuel cells (PEMFCs) are a promising technology that are set to contribute to achieving the current net carbon-emission neutrality targets.[1] If performance, cost and durability must be improved, one particular focus is on the electrocatalyst activity and long term durability for the sluggish oxygen reduction reaction (ORR). Platinum-rare earth metal alloys (Pt-REM) have been considered as suitable candidates to satisfy the ORR requirements,[2] and research on carbon-supported Pt-REM nanostructures has considerably increased in recent years.[3-11] Notwithstanding, their reported ORR activity is still lower than state-of-the-art carbon-supported PtNi and PtCo nanoalloys.[12, 13] Therefore, there is a need for a deeper understanding, especially during operation, of the relatively novel Pt-REM/C nanoalloys.

Recent studies using the rotating-disk electrode (RDE)[14-17] have indicated that the impact of early surface conditioning, *i.e.* electrochemical activation (ECA), has been hitherto underestimated, and is an important factor contributing to the performance of Pt-based

nanoalloys. For instance, Danisman *et al.*[17] have recently reported important activity changes of PtNiMo/C depending on the initial electrochemical surface pretreatment. Similar results have been reported for PtNi/C[15], PtCo/C[14] and PtCu/C[14, 16] nanocatalysts, Therefore, one might conclude that further studies are needed to understand the effect of the ECA on the ORR performance in more detail. Indeed, in our previous contribution[18], evolution of the crystal structure of hexagonal Pt-Nd/C nanoalloys during the ECA was observed for the first time for Pt-REM/C nanoalloys using *operando* wide-angle synchrotron X-ray scattering (WAXS) measurements. Briefly, the structural characterization of the as-prepared Pt-Nd/C electrocatalyst revealed that the crystal structure is *ca.* 100 *wt.%* the hexagonal Pt_5Nd phase, with compressive strain of *ca.* -3.7% relative to the Pt/C reference. However, it was determined from *operando* WAXS measurements that the first cathodic scan during the ECA (from open circuit potential to 0.05 V_{RHE}) triggers the growth of a Pt face-centred cubic (fcc) phase that reaches a stable weight fraction of *ca.* 20 *wt.%* (**Figure S4a**). From the trends of the individual scale factors and the average coherent domain sizes of these two components (hexagonal and fcc), **Figure S4b and S4c** respectively, it was surmised that the origin of the Pt fcc component might come from the electrochemical reduction of a Pt-containing amorphous phase. These striking results raised new questions concerning the origin and nature of the *actual* properties (structure, local coordination environment, chemical composition, morphology, particle size) of the stabilized electrocatalyst which describe the *real* beginning of life (BoL) state and are clearly different from the *ex situ* properties determined on the as-prepared nanomaterial. Furthermore, the characterization of the electrocatalyst properties after the ECA and before the ORR electrocatalytic evaluation is paramount for the understanding of the structure-activity-stability relationships of carbon supported Pt-REM nanoalloys as ORR electrocatalysts.

In this work, using the Pt-Nd/C nanocatalyst, the evolution of the structure, local electronic/coordination environment, and metal dissolution before, during and after the ECA (see **Supplementary Information S2**) were extracted from *in situ* X-ray absorption spectroscopy (XAS), *online* inductively coupled plasma mass spectrometry (ICP-MS), electron microscopy techniques (HAADF-STEM/EDX) and density functional theory (DFT), aiming to understand and properly characterize the *actual* BoL state of Pt-Nd/C before its electrocatalytic evaluation.

Firstly, the transient metal dissolution during the ECA protocol (**Supplementary Information S2**) was assessed using an electrochemical flow cell coupled with an ICP-MS[19] (**Supplementary Information S4**). The acquired specific dissolution profiles are shown in **Figure 1**. During the ECA, the results of **Figure 1a** indicate that the metal dissolution starts after polarizing the electrode from the open circuit potential (OCP) to the lower limit potential (0.05 V_{RHE}). One can also observe in **Figure 1a** that Pt dissolution starts slightly before than Nd dissolution, suggesting that the partial or total dissolution of the protective Pt layer triggers the Nd dissolution, with the most intense signal observed during the first cathodic scan. After that, the dissolution signal seems to be stabilized for both metals. The specific dissolution rate of Pt (pg_{dis} s^{-1} cm^{-2}_{Pt}) at the most intense dissolution peak is *ca.* 25-fold lower than that of Nd, despite Pt is 5 times greater abundant in the alloy stoichiometry. Indeed, after the partial or total dissolution of the protective smooth Pt layer at the surface and due to the larger atomic radii and surface energy of REM relative to Pt, it is expected that Nd atoms exposed at the surface/electrolyte interface are quickly oxidized into Nd^{3+} ($E^{0}_{Nd^{3+}/Nd^{0}}$ = -2.323 V_{SHE}) and dissolve once in contact with the acidic electrolyte, giving a strong thermodynamic driving force for the Nd segregation from the bulk of the alloy towards the surface. However, this process eventually induces the surface reconstruction and the expected thickening of the protective Pt-rich shell. Furthermore, the

dissolved Pt species might redeposit back through Oswald ripening,[19] forming longer Pt crystalline domains. These observations might suggest that the structural changes detected by WAXS are, until a certain extent, related to dissolution events. The total dissolved mass during the ECA, relative to the initial metal loading at the electrode, of Pt and Nd are 0.0029 ± 0.001 % and 1.78 ± 0.46 %, respectively.

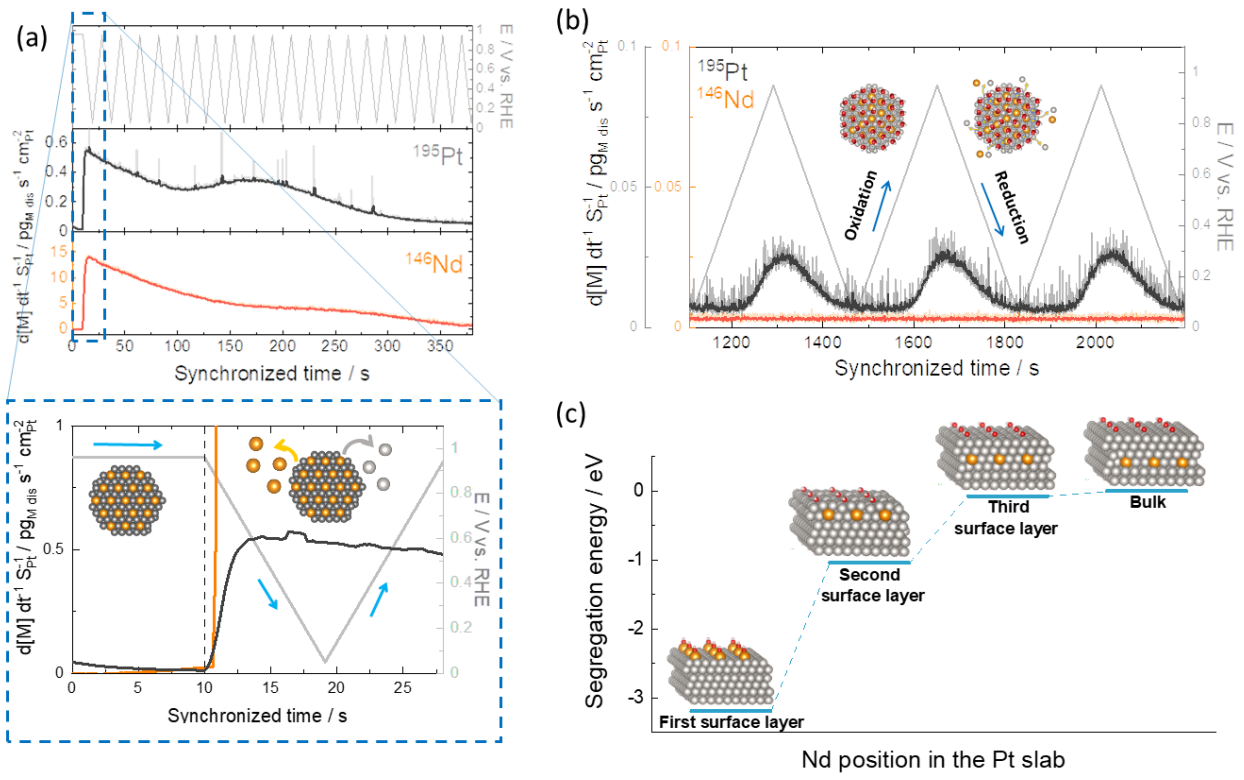

Figure 1. Transient dissolution profiles acquired from *online* ICP-MS analysis (a) during the electrochemical activation (20 cycles at 100 mV s^{-1}, the zoomed section shows the first dissolution events during the first potential cycle), and (b) during slow potentiodynamic cycles (3 cycles at 5 mV s^{-1}). (c) OH-adsorption induced segregation energy as function of the Nd position in the Pt slab. The negative values of segregation energies indicate the preference of Nd to segregate toward the surface.

It is known that the Pt dissolution is a transient process, *i.e.*, it depends on the potential scan rate (timescale).[20] To gain more information on the transient dissolution behaviour of Pt and Nd, three potentiodynamic cycles with slower potential scan rates (0.05 to 0.95 V_{RHE} at 5 mV s^{-1}) were applied following the ECA, see **Figure 1b**. The predominant Pt dissolution signal is centred in the cathodic scan, in agreement with the literature.[14, 19-23] This feature is a consequence of the reduction of the formed Pt oxide which induces a surface and sub-surface re-structuring *via* the place exchange mechanism,[14] being expected to gradually start at a critical coverage around or slightly below the potential of full coverage of chemisorbed oxygenated species.[20] Furthermore, dissolution of Nd seems to be suppressed. It may be concluded from this result that the surface and sub-surface re-structuring during the ECA triggers the stabilization of a thick protective Pt-rich shell, which prevents further Nd dissolution. With this knowledge, the OH-adsorption induced segregation energy was calculated as function of the Nd position in the Pt slab, *c.f.* **Figure 1c**, starting from Nd atoms exposed at the surface (first surface layer), Nd atoms protected by 1 Pt monolayer (second surface layer), Nd atoms protected by 2 Pt monolayers (third surface layer), and Nd atoms protected by 3 Pt monolayers (bulk). The aforementioned diagram clearly shows that, in presence of OH, Nd atoms located near the surface have strong tendency to segregate toward the top surface layer (the more negative the energy, the easier the segregation). However, the segregation of Nd atoms could be attenuated if they are protected by at least 3 Pt overlayers, resulting in a core/shell (Pt_5Nd alloy@Pt layers) system with a compressively strained Pt outer surface layer.[18]

Surface reconstruction is expected to modify the local electronic and coordination environments, and *in situ* XAS measurements were performed to investigate the local properties before and after the ECA, see **Figure 2a-c**. The spectra recorded *ex situ* were used for comparative purposes. It may be observed from the X-ray absorption near-edge structure (XANES) spectra at the Pt L_3 edge, *c.f.* **Figure 2a**, that the white line intensity follows the trend *ex situ* > before ECA > after ECA. This observation might indicate that the local electronic structure before and after the ECA differs from that in the as-prepared nanocatalyst, since the white line intensity is proportional to the number of empty Pt 5*d* states. Thus, the as-prepared sample is characterized by a higher density of unoccupied valence states (more vacancies) than the sample before and after the electrochemical conditioning. Nevertheless, the ECA also induces a lowering of the white line intensity, inferring a decreased surface oxidation state. This result might suggest that the surface oxides produced by the contact with air in the *ex situ* sample are reduced during operation, increasing the scale factor of the fcc phase observed in **Figure S4**. However, the redeposition of the dissolved Pt species *via* Oswald ripening might also occur simultaneously.[19] Therefore, the growing of the Pt fcc component could be related to the electrochemical reduction of the *ex situ* formed Pt oxides and the redeposition of dissolved Pt species.

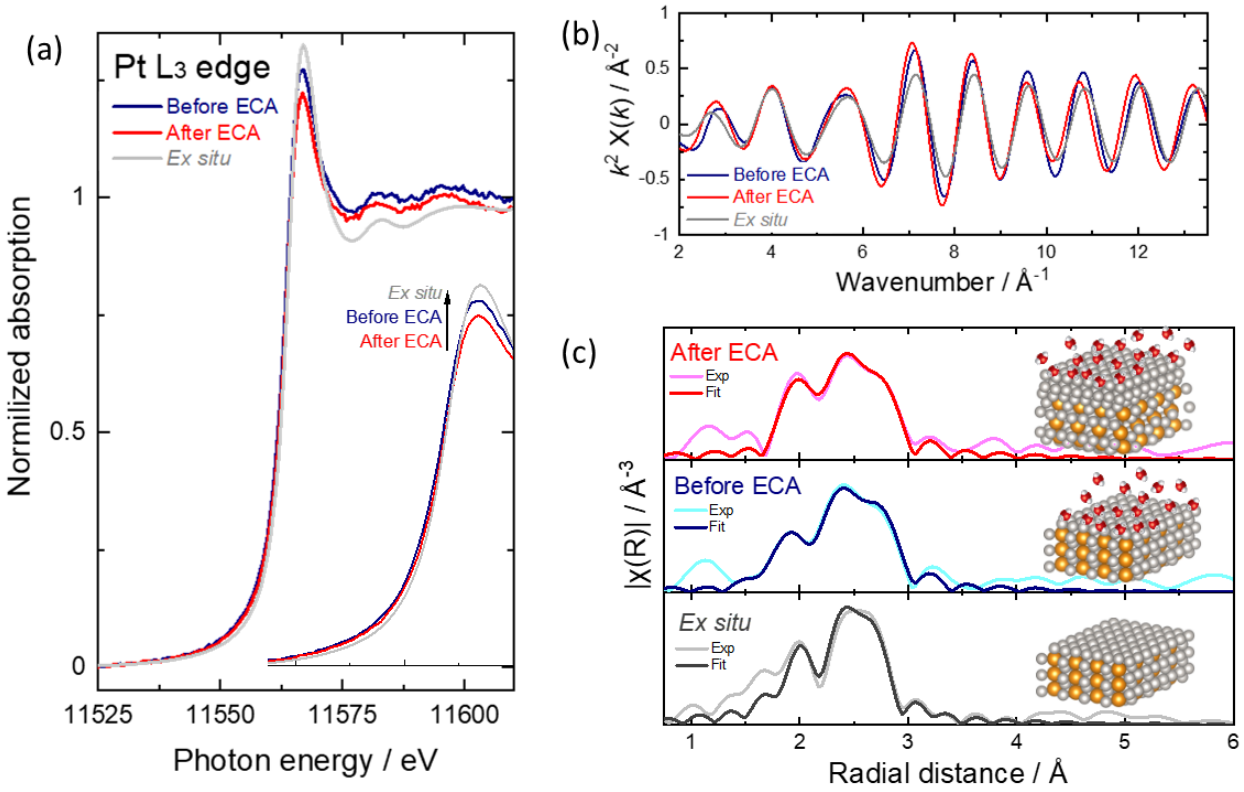

Figure 2. *In situ* Pt L_3 edge XAS measurements before (blue line) and after (red line) the electrochemical activation at the OCP: (a) XANES region and EXAFS fitting (b) in the *k*-space and (c) in the *R*-space. The *ex situ* spectra (grey line) is used as reference.

In the extended X-ray absorption fine structure (EXAFS) region in *k*-space, **Figure 2b**, the oscillations of the *ex situ* measurement are slightly modified before the ECA, and even stronger after the ECA. This feature could be related to adsorbates at the electrode/electrolyte interface[24] and surface re-structuring induced by the ECA, modifying the local coordination environment. The average first-shell Pt-Pt coordination number (N_{Pt-Pt}) and the average Pt-Pt bond lengths (R_{Pt-Pt}) were determined by fitting the filtered Fourier Transformed EXAFS spectra in the *R*-space shown in **Figure 2c** (fitting details are given in the **Supplementary Information S6**). When the Pt-Nd/C is in the electrochemical environment, *i.e.*, before and after the ECA, the N_{Pt-}

158 $_{Pt}$ increases from 5.6 (*ex situ*) to 7.6 (before ECA) and 8.05 (after ECA). This result might
159 indicate the formation of larger Pt domains before and after the ECA, in line with the growth of
160 the Pt fcc phase observed by WAXS. The average $R_{Pt\text{-}Pt}$ before the ECA is larger than in the *ex*
161 *situ* as- prepared catalyst, increasing from 2.66 Å to 2.69 Å. This observation is consistent with
162 the slight increase in coordination number and might also be related to the effect of adsorbates on
163 the crystal lattice expansion.[25] After the ECA, the $R_{Pt\text{-}Pt}$ decreases to 2.67 Å, which still reflects
164 an expansion with respect to the measured *ex situ* value, being in line with our previous WAXS
165 results.[18] Owing to the fact that the specific ORR activity of Pt-REM presents an exponential
166 dependence on the surface compressive strain,[26, 27] these results clearly underpin that an
167 overestimated *ex situ* strain magnitude might not properly describe the ORR electrochemical
168 activity, since the induced strain evolves during operation.[25]

169 After the ECA in the *online* ICP-MS set up, the catalyst layer was recovered to examine the
170 nanocatalyst structure and its chemical profile by HAADF-STEM/EDX, *c.f.* **Figure 3**. In fact,
171 the average size of the NPs and agglomerates after the ECA, shown in the **Supplementary**
172 **Information S8,** is *ca.* 7 nm and 13 nm, *i.e.* no significant difference to the values in the as-
173 prepared electrocatalyst.

174

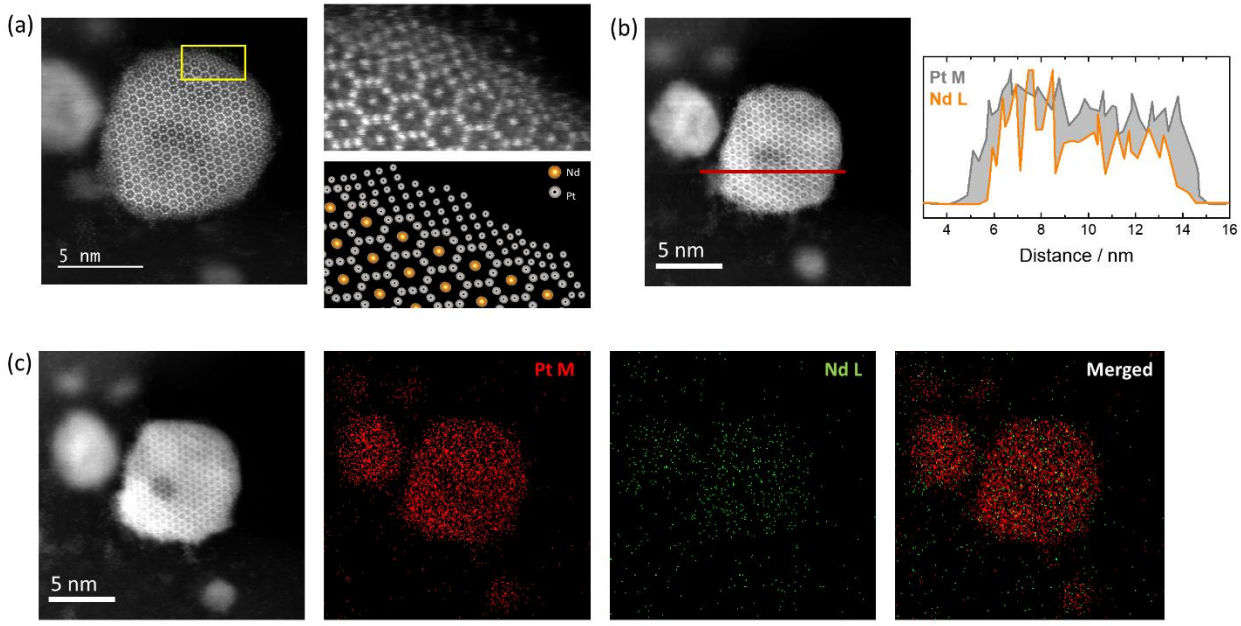

Figure 3. HAADF-STEM analysis after the electrochemical activation: (a) representative atomic-resolution micrograph with an overview at the NP border and its respective atomic simulation, (b) chemical line scan by EDX, and (c) chemical mapping by EDX.

The atomic-resolution micrograph of the electrocatalyst shown in **Figure 3a** clearly confirms the presence of the hexagonal Pt_5Nd alloy after the ECA, in agreement with the previous WAXS results. However, a Pt-rich atomic shell, which is ~ 5-6 atoms thick, is clearly observed for the isolated NP (**Figure 3a**), in agreement with the EDX line scan (**Figure 3b**) and EDX chemical mapping (**Figure 3c**) of the NP. These results support the thickening of the protective Pt overlayers after ECA due to the surface reconstruction. Different regions of the sample were analyzed by EDX, observing higher Pt:Nd ratios (**Supplementary Information S8**). Our proposed model derived from DFT[18] suggests that as the Pt shell thickness increases (higher number of Pt layers over the Pt_5Nd core) the Pt-Pt interatomic distances through the *z*-axis increase (lattice dilatation), while the surface Pt atoms are compressively strained laterally, along the *x*-*y* plane. The average residual strain is approximately -0.89 %, suggesting a counterbalance

between compressive and tensile strain. Indeed, the projected density of states (PDOS) of a Pt monolayer onto the Pt_5Nd alloy (Pt_5Nd@Pt) presents more empty states than the structure with 5 Pt layers onto the Pt_5Nd alloy (Pt_5Nd@5-Pt), see **Supplementary Information S10**. This result, supported by the XANES and HAADF-STEM studies, clearly suggests that the electronic structure of the as-prepared catalyst evolves once the surface conditioning is performed, modifying its electrocatalytic properties.

In conclusion, the transition of the properties of carbon-supported hexagonal Pt-Nd nanoalloys occurring during the electrochemical activation was studied by *online* ICP-MS, *in situ* XAS and atomic-resolution HAADF-STEM combined with DFT calculations. The results of the study suggest that the structural transitions during the early electrochemical activation are consequence of the electrochemical reduction of the *ex situ* formed oxides and metal dissolution. This metal dissolution promotes surface restructuring, and thickening of the initial protective Pt-rich shell to 5-6 atoms thick. However, the compressive strain in the restructured surface is attenuated compared to that determined in the *ex situ* measurement. The *ex situ* strain magnitude does not properly describe the ORR electrochemical activity, since the induced strain evolves during activation.

Therefore, the stabilized properties after the electrochemical activation should be taken into consideration when discussing the electrocatalyst beginning of life state for the structure-activity-stability relationships rather than those measured *ex situ* on the as-synthesized electrocatalyst, as well as in the analysis of long-term *in situ/operando* accelerated degradation tests.

AUTHOR INFORMATION

Corresponding Authors

* *Carlos A. Campos-Roldán*

Email: carlos-augusto.campos-roldan@umontpellier.fr

**Sara Cavaliere*

Email: sara.cavaliere@umontpellier.fr

ORCID

C.A. Campos-Roldán: 0000-0002-1517-9037

J.-S. Filhol: 0000-0002-3681-9267

H. Guesmi: 0000-0002-9369-523X

R. Chattot: 0000-0001-6169-530X

A. Zitolo: 0000-0002-2187-6699

P.-Y. Blanchard: 0000-0003-1659-6868

J. Rozière: 0000-0001-6211-5047

D.J. Jones: 0000-0003-3787-2462

S. Cavaliere: 0000-0003-0939-108X

Author Contributions

The manuscript was written through contributions of all authors. All authors have given approval to the final version of the manuscript.

Author Contributions

Carlos A. Campos-Roldán: Conceptualization, methodology, writing-original draft, formal analysis, investigation, **Jean-Sébastien Filhol**: Writing-review & editing, formal analysis, methodology, **Hazar Guesmi**: Writing-review & editing, formal analysis, methodology, **Mickaël Bigot**: Investigation, **Raphaël Chattot**: Writing-review & editing, conceptualization, investigation, **Andrea Zitolo**: Writing-review & editing, investigation, **Pierre-Yves Blanchard**: Writing-review & editing, supervision, **Jacques Rozière**: Writing-review & editing, conceptualization, funding acquisition, supervision, **Deborah J. Jones**: Writing-review & editing, conceptualization, funding acquisition, supervision, **Sara Cavaliere**: Writing-review & editing, conceptualization, funding acquisition, supervision

ASSOCIATED CONTENT

The following files are available free of charge.

Supporting Information: Synthesis procedure, electrochemical protocol, details regarding the measurements, comparison of the electrochemical signal between the used setups, supplementary methodology information are available in the Supporting Information.

ACKNOWLEDGEMENTS

The research leading to these results has received funding from the HIGHLANDER and IMMORTAL projects, which receive funding from the Clean Hydrogen Partnership under grant agreement numbers 101101346 and 101006641 respectively. This Joint

Undertaking receives support from the European Union's Horizon Europe research and innovation programme, Hydrogen Europe and Hydrogen Europe Research. R.C received financial support from the French National Research Agency through the HOLYCAT project (grant number n◦ ANR-22-CE05-0007). We acknowledge Synchrotron SOLEIL (Gif-sur Yvette, France) for provision of synchrotron radiation facilities at beamline SAMBA under the proposal number 20211337. We also thank Dr. Vincent Collière from Centre de Microcaractérisation Raimond Castaing de Toulouse (UAR3623), and Dr. Nuria Romero and Dr. Karine Philippot from the Laboratoire de Chimie de Coordination of the Université de Toulouse for their assistance with the electron microscopy characterization.

REFERENCES

1. van der Spek, M.; Banet, C.; Bauer, C.; Gabrielli, P.; Goldthorpe, W.; Mazzotti, M.; Munkejord, S. T.; Røkke, N. A.; Shah, N.; Sunny, N.; Sutter, D.; Trusler, J. M.; Gazzani, M., Perspective on the hydrogen economy as a pathway to reach net-zero CO_2 emissions in Europe. *Energy Environ. Sci.* **2022,** *15* (3), 1034-1077.
2. Escudero-Escribano, M.; Malacrida, P.; Hansen, M.; Vej-Hansen, U.; Velázquez-Palenzuela, A.; Tripkovic, V.; Schiøtz, J.; Rossmeisl, J.; Stephens, I.; Chorkendorff, I., Tuning the activity of Pt alloy electrocatalysts by means of the lanthanide contraction. *Science* **2016,** *352* (6281), 73-76.
3. Campos- Roldán, C. A.; Jones, D. J.; Rozière, J.; Cavaliere, S., Platinum- Rare Earth Alloy Electrocatalysts for the Oxygen Reduction Reaction: A Brief Overview. *ChemCatChem* **2022,** *14* (19), e202200334.
4. Campos-Roldán, C. A.; Parnière, A.; Donzel, N.; Pailloux, F.; Blanchard, P.-Y.; Jones, D. J.; Rozière, J.; Cavaliere, S., Influence of the Carbon Support on the Properties of Platinum–Yttrium Nanoalloys for the Oxygen Reduction Reaction. *ACS Applied Energy Materials* **2022,** *5* (3), 3319-3328.
5. Campos-Roldán, C. A.; Pailloux, F.; Blanchard, P.-Y.; Jones, D. J.; Rozière, J.; Cavaliere, S., Rational Design of Carbon-Supported Platinum–Gadolinium Nanoalloys for Oxygen Reduction Reaction. *ACS Catal.* **2021,** *11* (21), 13519-13529.
6. Campos-Roldan, C. A.; Pailloux, F.; Blanchard, P. Y.; Jones, D. J.; Roziere, J.; Cavaliere, S., Enhancing the activity and stability of carbon-supported platinum-gadolinium nanoalloys towards the oxygen reduction reaction. *Nanoscale Adv* **2021,** *4* (1), 26-29.

7. Gunji, T.; Tanaka, S.; Inagawa, T.; Otsuka, K.; Matsumoto, F., Atomically Ordered Pt_5La Nanoparticles as Electrocatalysts for the Oxygen Reduction Reaction. *ACS Appl. Nano Mater.* **2022,** *5* (4), 4958-4965.
8. Hu, Y.; Jensen, J. O.; Cleemann, L. N.; Brandes, B. A.; Li, Q., Synthesis of Pt-Rare Earth Metal Nanoalloys. *J Am Chem Soc* **2020,** *142* (2), 953-961.
9. Itahara, H.; Takatani, Y.; Takahashi, N.; Kosaka, S.; Nagoya, A.; Inaba, M.; Kamitaka, Y.; Morimoto, Y., Synthesis of Carbon-Supported Intermetallic Pt_5Ce Compound Nanoparticles via a Water-Based Impregnation Route. *Chem. Mater.* **2021,** *34* (1), 422-429.
10. Xu, S.-L.; Zhao, S.; Zeng, W.-J.; Li, S.; Zuo, M.; Lin, Y.; Chu, S.; Chen, P.; Liu, J.; Liang, H.-W., Synthesis of a Hexagonal-Phase Platinum–Lanthanide Alloy as a Durable Fuel-Cell-Cathode Catalyst. *Chemistry of Materials* **2022,** *34* (23), 10789-10797.
11. Zhou, Q.; Jensen, J. O.; Cleemann, L. N.; Li, Q.-F.; Hu, Y., Tailoring the particle sizes of Pt_5Ce alloy nanoparticles for the oxygen reduction reaction. *Advanced Sensor and Energy Materials* **2022,** *1* (3), 100025-100033.
12. Ahn, C. Y.; Park, J. E.; Kim, S.; Kim, O. H.; Hwang, W.; Her, M.; Kang, S. Y.; Park, S.; Kwon, O. J.; Park, H. S.; Cho, Y. H.; Sung, Y. E., Differences in the Electrochemical Performance of Pt-Based Catalysts Used for Polymer Electrolyte Membrane Fuel Cells in Liquid Half- and Full-Cells. *Chem Rev* **2021,** *121* (24), 15075-15140.
13. Borup, R. L.; Kusoglu, A.; Neyerlin, K. C.; Mukundan, R.; Ahluwalia, R. K.; Cullen, D. A.; More, K. L.; Weber, A. Z.; Myers, D. J., Recent developments in catalyst-related PEM fuel cell durability. *Curr Opin Electrochem* **2020,** *21*, 192-200.
14. Gatalo, M.; Jovanovič, P.; Petek, U.; Šala, M.; Šelih, V. S.; Ruiz-Zepeda, F.; Bele, M.; Hodnik, N.; Gaberšček, M., Comparison of Pt–Cu/C with Benchmark Pt–Co/C: Metal Dissolution and Their Surface Interactions. *ACS Applied Energy Materials* **2019,** *2* (5), 3131-3141.
15. Chattot, R.; Roiron, C.; Kumar, K.; Martin, V.; Campos Roldan, C. A.; Mirolo, M.; Martens, I.; Castanheira, L.; Viola, A.; Bacabe, R.; Cavaliere, S.; Blanchard, P.-Y.; Dubau, L.; Maillard, F.; Drnec, J., Break-In Bad: On the Conditioning of Fuel Cell Nanoalloy Catalysts. *ACS Catalysis* **2022,** *12* (24), 15675-15685.
16. Alekseenko, A. A.; Pavlets, A. S.; Belenov, S. V.; Safronenko, O. I.; Pankov, I. V.; Guterman, V. E., The electrochemical activation mode as a way to exceptional ORR performance of nanostructured PtCu/C materials. *Applied Surface Science* **2022,** *595*, 153533.
17. Danisman, B.; Zhang, G. R.; Baumunk, A. F.; Yang, J.; Brummel, O.; Darge, P.; Mayrhofer, K. J. J.; Libuda, J.; Ledendecker, M.; Etzold, B. J. M., Strong Activity Changes Observable during the First Pretreatment Cycles of Trimetallic PtNiMo/C Catalysts. *ChemElectroChem* **2023,** *10* (16).
18. Campos-Roldán, C. A.; Chattot, R.; Filhol, J.-S.; Guesmi, H.; Pailloux, F.; Bacabe, R.; Blanchard, P.-Y.; Zitolo, A.; Drnec, J.; Jones, D. J.; Cavaliere, S., Structure Dynamics of Carbon-Supported Platinum-Neodymium Nanoalloys during the Oxygen Reduction Reaction. *ACS Catalysis* **2023,** *13* (11), 7417-7427.
19. Dukic, T.; Pavko, L.; Jovanovic, P.; Maselj, N.; Gatalo, M.; Hodnik, N., Stability challenges of carbon-supported Pt-nanoalloys as fuel cell oxygen reduction reaction electrocatalysts. *Chem Commun (Camb)* **2022,** *58* (100), 13832-13854.
20. Topalov, A. A.; Cherevko, S.; Zeradjanin, A. R.; Meier, J. C.; Katsounaros, I.; Mayrhofer, K. J. J., Towards a comprehensive understanding of platinum dissolution in acidic media. *Chem. Sci.* **2014,** *5* (2), 631-638.

21. Sandbeck, D. J. S.; Inaba, M.; Quinson, J.; Bucher, J.; Zana, A.; Arenz, M.; Cherevko, S., Particle Size Effect on Platinum Dissolution: Practical Considerations for Fuel Cells. *ACS Appl Mater Interfaces* **2020,** *12* (23), 25718-25727.
22. Fuchs, T., Drnec, J., Calle-Vallejo, F., Stubb, N., Sandbeck, D., Ruge, M., Cherevko, S., Harrington, D., Magnussen, O., Structure dependency of the atomic-scale mechanisms of platinum electro-oxidation and dissolution. *Nat Catal* **2020,** *3*, 754-761.
23. Dukic, T.; Moriau, L. J.; Pavko, L.; Kostelec, M.; Prokop, M.; Ruiz-Zepeda, F.; Sala, M.; Drazic, G.; Gatalo, M.; Hodnik, N., Understanding the Crucial Significance of the Temperature and Potential Window on the Stability of Carbon Supported Pt-Alloy Nanoparticles as Oxygen Reduction Reaction Electrocatalysts. *ACS Catal* **2022,** *12* (1), 101-115.
24. Gomes, B. F.; Prokop, M.; Bystron, T.; Loukrakpam, R.; Melke, J.; Lobo, C. M. S.; Fink, M.; Zhu, M.; Voloshina, E.; Kutter, M.; Hoffmann, H.; Yusenko, K. V.; Buzanich, A. G.; Röder, B.; Bouzek, K.; Paulus, B.; Roth, C., Following Adsorbed Intermediates on a Platinum Gas Diffusion Electrode in H3PO3-Containing Electrolytes Using In Situ X-ray Absorption Spectroscopy. *ACS Catalysis* **2022,** *12* (18), 11472-11484.
25. Chattot, R.; Martens, I.; Mirolo, M.; Ronovsky, M.; Russello, F.; Isern, H.; Braesch, G.; Hornberger, E.; Strasser, P.; Sibert, E.; Chatenet, M.; Honkimaki, V.; Drnec, J., Electrochemical Strain Dynamics in Noble Metal Nanocatalysts. *J Am Chem Soc* **2021,** *143* (41), 17068-17078.
26. Hernandez-Fernandez, P.; Masini, F.; McCarthy, D. N.; Strebel, C. E.; Friebel, D.; Deiana, D.; Malacrida, P.; Nierhoff, A.; Bodin, A.; Wise, A. M.; Nielsen, J. H.; Hansen, T. W.; Nilsson, A.; Stephens, I. E.; Chorkendorff, I., Mass-selected nanoparticles of Pt_xY as model catalysts for oxygen electroreduction. *Nat Chem* **2014,** *6* (8), 732-8.
27. Velázquez-Palenzuela, A.; Masini, F.; Pedersen, A. F.; Escudero-Escribano, M.; Deiana, D.; Malacrida, P.; Hansen, T. W.; Friebel, D.; Nilsson, A.; Stephens, I. E. L.; Chorkendorff, I., The enhanced activity of mass-selected Pt_xGd nanoparticles for oxygen electroreduction. *J. Catal.* **2015,** *328*, 297-307.

TOC graphic